

Turbulent electromagnetic fields at sub-proton scales: two-fluid and full-kinetic plasma simulations

C.A. González,^{1, a)} T. Parashar,² D. Gomez,³ W.H. Matthaeus,² and P. Dmitruk¹

¹⁾*Departamento de Física, Facultad de Ciencias Exactas y Naturales, Universidad de Buenos Aires and IFIBA, CONICET, Ciudad universitaria, 1428 Buenos Aires, Argentina.*

²⁾*Bartol Research Institute and Department of Physics and Astronomy, University of Delaware, Newark, Delaware, USA*

³⁾*Instituto de Astronomía y Física del Espacio, CONICET-UBA, Ciudad Universitaria, 1428 Buenos Aires, Argentina*

Plasma dynamics is a multi-scale problem that involves many spatial and temporal scales. Turbulence connects the disparate scales in this system through a cascade that is established by nonlinear interactions. Most astrophysical plasma systems are weakly collisional, making a fully kinetic Vlasov description of the system essential. Use of reduced models to study such systems is computationally desirable but careful benchmarking of physics in different models is needed. We perform one such comparison here between fully kinetic Particle-In-Cell (PIC) model and a two-fluid model that includes Hall physics and electron inertia, with a particular focus on the sub-proton scale electric field. We show that in general the two fluid model captures large scale dynamics reasonably well. At smaller scales the Hall physics is also captured reasonably well by the fluid code but electron features show departures from the fully kinetic model. Implications for use of such fluid models are discussed.

I. INTRODUCTION:

Turbulence is generally defined as an ensemble of broadband fluctuations that arise from the nonlinear interaction among many degrees of freedom, which involves the energy transfer between scales. In hydrodynamic flows, energy is transferred or cascaded from large to progressively smaller scales where it is finally dissipated. The corresponding energy spectrum displays a Kolmogorov power-law¹⁻³ that represents scale invariance in a given range. The large-scale behavior of turbulent plasmas, traditionally described within the framework of magnetohydrodynamics, is also characterized by a direct energy cascade. The nature of this cascade and the corresponding effect on plasma heating are important problems in solar and space physics. The dynamics of these plasmas are complex, with many temporal and spatial scales simultaneously involved. For instance, the energy transfer processes that occur at proton and electron inertial scales in collisionless plasmas, involve coherent features such as tube-like structures⁴⁻⁷ and intermittent events that emerge⁸⁻¹¹ through the coupling between scales. These processes are also related to the production of high energetic particle populations¹²⁻¹⁵.

In-situ observation of the solar wind has allowed research to go deeper into the physics of plasma turbulence. In spite of the progressively higher resolution cadence of recent space missions, there is still a debate about the characteristics of the turbulence near the dissipation range. The solar wind displays a Kolmogorov-like

power-law at inertial range. However, when approaching the proton inertial scale, the magnetic energy spectrum displays a break^{16,17} toward a somewhat steeper power law. The spectral index at proton scales can vary depending on the physical processes acting on the flow, such as magnetic reconnection¹⁸⁻²⁰, damping of kinetic Alfvén waves (KAWs), anisotropies in the proton distribution function or differential particle heating. The details of the energy cascade beyond the electron inertial range is even less understood, although observations show a much steeper magnetic energy spectrum. There is still no agreement in the plasma physics community about the dominant dissipation mechanisms at these small scales^{21,22}. For instance, finite electron larmor effects^{23,24}, electron-cyclotron resonance, magnetosonic, whistler and/or KAW mode turbulence²⁵⁻³² are some of the likely candidates to mediate the energy transfer and dissipation at electron scales.

Solar wind observation evidence that the magnetic and electric field spectra are well correlated on the inertial range, and this correlation is in agreement with the scenario of Alfvénic turbulence³³. It is well established that there is a transition from MHD turbulence to kinetic turbulence, where the electric and magnetic field spectra depart each other at around proton scales, with a relatively more intense electric field and with a shallower slope^{34,35}. *In-situ* measurements^{25,26,28} are in agreement with theoretical predictions³⁶ about the kinetic Alfvén and whistler regimes at proton and electron inertial scales, where a parallel electric field component is generated. The importance of the parallel electric field fluctuations is due to the relevance of Landau damping and the wave-particle interaction that might become significant at kinetic scales in turbulent plasmas³⁷.

^{a)}Electronic mail: caangonzalez@df.uba.ar

From a theoretical point of view, the dynamics of plasmas and their self-consistent electric and magnetic fields can alternatively be described by multi-fluid or kinetic descriptions. According to the more fundamental kinetic approach, the dynamics is described by the Vlasov equation for each plasma species, coupled with Maxwell's equations for the electric and magnetic fields. The relatively simpler multi-fluid models are derived from the moments of the Vlasov equation and the plasma dynamics for each species is described by fluid quantities such as its density, velocity field and pressure. There are several different numerical methods based on fluid-like descriptions, depending on the physical processes involved. In the case of magnetohydrodynamics (MHD) the dynamics is described by a single fluid. Other fluid based methods include, but are not limited to Hall-MHD³⁸, Electron MHD^{39,40}, Electron Reduced MHD³⁶, Electron inertial Hall-MHD⁴¹, Hall-Finite Larmor Radius MHD^{42,43} and Landau-Fluid^{44,45}.

There are also numerical methods based on a full kinetic description^{46,47}, often constrained by computational limitations. One possibility is to integrate the Vlasov equation for the dynamics of each species, coupled to Maxwell's equations for the electric and magnetic fields⁴⁷. There is also the case of full kinetic particle-in-cell method (PIC) where the plasma species, both ions and electrons, are treated as computational macroparticle which represents a number of real particles with similar physical properties and in a close region of the phase space^{48,49}. Besides fluid and kinetic methods, there are other hybrid methods that typically consider the electrons as a fluid and kinetic protons or variations of that.⁵⁰

In this paper we perform a comparison between a two-fluid and a full PIC simulation where the dynamics of both protons and electrons and the corresponding inertial scales have been taken into account. The comparison made in this work can be considered within the framework of the “*Turbulent dissipation challenge*”²², in the spirit of comparing different simulation models under the same initial conditions with similar physical and numerical parameters despite the limitations of each numerical and theoretical framework. Several attempts to compare different numerical methods have been carried out in recent years^{51–55} and it has resulted in a very useful and interesting approach to explore different physical mechanisms in plasma turbulence.

While in the two-fluid simulation the system is driven by the dynamics of the flow, the PIC simulation allows for the interaction between the field and individual macroparticles, thus enabling new channels for the exchange of energy^{56–60}. Also, many physical questions must be addressed in order to shed light on the importance of intermittency, high and low-frequency wave phenomena and particle heating on dissipation processes in collisionless plasmas. The goal of this paper is to delve more deeply into the relationship between large-scale and kinetic scale fluctuations, noting both similarities and differences in two very different plasma models. In particu-

lar, we explore contributions to the electric field at sub-proton scales where kinetic contributions may strongly influence dissipation and charged particle energization.

This paper has the following organization: in section II. we present the kinetic and the two-fluid models. In section III we describe the initialization setup for both simulations and introduce the relevant plasma parameters. In section IV. we present the results of the simulation. First, we compare important macroscopic quantities for both simulations, like flow energy, current density and the magnetic field. After that, we study the electric field at different spatial scales for both simulations, comparing the various terms of the generalized Ohm's law with the aim to unveil which terms are dominant at sub-proton scales. Conclusions and directions for future work are established in Section V.

II. MODELS:

This section describes the models employed for this study. We consider a collisionless approximation where the dynamics of each species s is governed by the kinetic Vlasov equation:

$$\frac{\partial f_s}{\partial t} + \mathbf{v} \cdot \nabla f_s + \frac{q_s}{m_s} \left(\mathbf{E} + \frac{\mathbf{v} \times \mathbf{B}}{c} \right) \cdot \frac{\partial f_s}{\partial \mathbf{v}} = 0 \quad (1)$$

The evolution of the distribution function $f_s(\mathbf{r}, \mathbf{v}, t)$ for the plasma species s with a given charge q_s and mass m_s depends on the external and self-consistent electromagnetic fields \mathbf{E} and \mathbf{B} , that follow Maxwell's equations:

$$\frac{\partial \mathbf{E}}{\partial t} = c \nabla \times \mathbf{B} - 4\pi \mathbf{J}, \quad \frac{\partial \mathbf{B}}{\partial t} = -c \nabla \times \mathbf{E} \quad (2)$$

$$\nabla \cdot \mathbf{E} = 4\pi \rho, \quad \nabla \cdot \mathbf{B} = 0 \quad (3)$$

The sources of Equations (2) and (3) (i.e. the charge density ρ and the electric current density \mathbf{J}) are obtained directly from the distribution function of all plasma species through: $\mathbf{J} = \sum_s q_s \int \mathbf{v} f_s d^3 \mathbf{r}$ and $\rho = \sum_s q_s \int f_s d^3 \mathbf{r}$.

On the other hand, the fluid model adopted for this paper is a two-fluid MHD, that extends MHD to include the dynamics of both protons and electrons. The model contains the momentum equation for the both species ($s = e, i$):

$$m_s n \frac{d\mathbf{u}_s}{dt} = q_s n \left(\mathbf{E} + \frac{\mathbf{u}_s \times \mathbf{B}}{c} \right) - \nabla p_s + \mu_s \nabla^2 \mathbf{u}_s \pm \mathbf{R} \quad (4)$$

With the total derivative $d/dt = \partial/\partial t + \mathbf{u}_s \cdot \nabla$, the pressure p_s , \mathbf{u}_s is the velocity field and μ_s is the viscosity for a given plasma species. \mathbf{R} is the rate of momentum exchanged between protons and electron through collisions and it is assumed to be proportional to the relative

speed between plasma species $R = -nm_i\nu_{ie}(\mathbf{u}_i - \mathbf{u}_e)$, where ν_{ie} is the collisional frequency of an ion against electrons. Note that although in the fluid model the collisions between plasma species must be taken into account since it determines the smallest timescale in the model, we are interested in studying and comparing collisionless phenomena at relatively larger scales. Therefore, we restrict ourselves to examination of quantities that relate to spatial and temporal scales common to both models.

We are interested in studying the non-relativistic limit, and so the displacement current can be neglected. Then the current density can be written as follows:

$$\mathbf{J} = \frac{c}{4\pi} \nabla \times \mathbf{B} = en(\mathbf{u}_i - \mathbf{u}_e) \quad (5)$$

$$n_i = n_e = n \quad \nabla \cdot \mathbf{u}_{i,e} = 0 \quad (6)$$

We assume quasi-neutrality and incompressibility for both proton and electron fluids (Equations. (6)). We refer the reader to Andres et al. (2014) paper for a complete description of the two-fluid model. This fluid model, where the electron mass is not neglected, has been called EIHMHD, for electron inertia Hall MHD⁴¹.

An expression for the electric field emerges from the electron momentum equation, leading to the generalized Ohm's law^{50,61,62}:

$$\mathbf{E} = -\mathbf{U} \times \mathbf{B} + \frac{1}{n} \mathbf{J} \times \mathbf{B} - \frac{1}{n} (\nabla p_e + \nabla \cdot \Pi_e) - \frac{d_e^2}{n} \frac{\partial \mathbf{J}}{\partial t} + \eta \mathbf{J} \quad (7)$$

With $\mathbf{U} = \frac{(m_i \mathbf{u}_i + m_e \mathbf{u}_e)}{(m_i + m_e)}$ the bulk velocity, $p = \frac{1}{3} P_{ii}$ and $\Pi_{ij} = P_{ij} - p\delta_{ij}$, one may conveniently decompose the electron pressure tensor into isotropic and deviatoric parts. Equation (7) is a normalized version of the electric field in units of the proton inertial length $d_i = c/\omega_{pi}$ and Alfvén velocity $v_A = B_0/(4\pi nm_i)^{1/2}$, appropriate for a magnetized plasma. The RHS terms are the induction (ideal MHD) term, the Hall term (related to differential flow of ions and electrons), which is important at scales $< d_i$. The isotropic and anisotropic electron pressure terms are also important at scales smaller than d_i . The electron inertial term becomes relevant at electron inertial length $d_e = c/\omega_{pe} = \sqrt{m_e/m_i} d_i$. Those terms deal with frequencies much lower than the electron plasma frequency and could mediate some phenomena that occur on sub-proton scales⁶³. The last term is the contribution to the electric field that results from collisional resistivity. Ohm's law is valid for a system size larger than the Debye length ($L \gg \lambda_D$) and for plasma frequencies slower than the electron plasma frequency ($\omega \ll \omega_{pe}$). At scales smaller than λ_D and frequencies greater than ω_{pe} , the quasi-neutrality condition becomes invalid. The validity of this equation is also constrained to a weakly magnetized plasma ($\omega_{ce} \ll \omega_{pe}$) with $\omega_{ce} = eB/m_e c$ the electron cyclotron frequency around the mean magnetic

field. It is extremely difficult to simulate such values in fully kinetic models as the simulations become prohibitively expensive in this regime. Typical fully kinetic simulations have $\omega_{ce}/\omega_{pe} \sim 3$ or so.

III. SIMULATION SETUP AND THE INITIAL CONDITIONS

The simulations presented in this paper are in 2.5D dimensions (two-dimensional dependence and all three components of the field vectors). We use periodic boundary conditions with an out-of-plane mean magnetic field B_0 for both kinetic and two-fluid simulations. The kinetic simulation is performed with the electromagnetic PIC code P3D⁶⁴. This is a finite difference particle code, where the particles are advanced using the Boris scheme and the Maxwell's equations are advanced an explicit trapezoidal leapfrog algorithm. The two-fluid simulation is done employing a Fourier pseudospectral code with a second-order Runge-Kutta time integration scheme. The system size in the PIC simulation has $L = L_x = L_y = 149.6d_i$ with $N_x = N_y = 4096$ number of grid points. Here, we study plasma with initial ion and electron temperature equilibrium ($T_i/T_e = 1$), with a mass ratio $m_e/m_i = 0.04$ and $\beta_e = \beta_i = 0.6$. The proton scale is at $k_{d_i} \sim 23.8k_{box}$, the electron scale appears at $k_{d_e} \sim 120k_{box}$ and the Debye length is at $k_{\lambda_D} = 652k_{box}$, where k_{box} is the wave-number corresponding to the largest wavelength that can fit in the box in the PIC simulation. With the above mentioned parameters we capture the MHD-like behavior that results self-consistently in kinetic simulations⁶⁵.

The system size must be large enough to represent the energy evolution expected in the MHD simulation and the development of a broad inertial range in the spectrum. The PIC simulations are also susceptible to noise effects due to the statistics in the number of macro particles per grid cell (ppc) used in the simulations. The number of ppc is important for the fields accuracy at Debye length where the thermalization may have a dramatic effect on the features of kinetic simulations^{66,67}. We use 3200 ppc in order to reduce those effects on the Debye scale and compare the entire evolution with the two-fluid simulation where the Debye length is not resolved.

The two-fluid simulation is in a normalized square box of length $L = 2\pi L_0$, where L_0 is the characteristic length (also called energy containing scale) defined as $L_0 = \int (E(k)/k) dk / \int E(k) dk$ with $E(k)$ the energy spectral density at wavenumber k . To suppress the aliasing effects, the code uses a maximum wavenumber $k_{max} = N/3$ where N is the Fourier modes resolution in the simulation. For this simulation, we used a resolution of 2048 Fourier modes, with equal viscosity and resistivity ($\eta = \nu = 7.5 \times 10^{-6}$). With the same mass ratio used in PIC simulation ($m_e/m_i = 0.04$), the corresponding proton scale is at $k_{d_i} \sim 25$ in the simulation, the electron scale appears at $k_{d_i} \approx 125$ and the dissipation scale is

$k_{diss} = 356$. $k_{diss} = \langle j^2 + w^2 \rangle^{1/4} / \sqrt{\mu}$. is the viscous dissipation scale that depends on the energy dissipation rate and the viscosity of the flow. That scale lacks physical sense for collisionless plasmas and for kinetic models where the energy dissipation is due to other phenomena.

Our goal in the following sections is to compare the results arising from these two descriptions, restricting ourselves to the scales that both models share in common. We have done freely decaying turbulence simulations and the initial conditions are chosen such that the root mean square (rms) of magnetic fluctuation $\langle \mathbf{b} \rangle / B_0 = 1/3.16$, and the Alfvén ratio of fluctuating kinetic and magnetic energies is $E_v/E_b = 1$. We initially excite a shell in k -space with wavenumber $2 \leq |\mathbf{k}| \leq 4$, with a specified spectral shape and Gaussian random phases.

As those codes represent different plasma models with different normalization scheme, in order to compare the results of kinetic and two-fluid simulation, we take as a common characteristic timescale the nonlinear time (or eddy turnover time) defined as $t_{nl} = L/\delta u$, with δu the (r.m.s) velocity value and L the system size for each simulation.

IV. RESULTS:

In Figure 1 we present some global quantities for both fluid and kinetic simulations. The upper panel describes the time evolution of the energy per unit mass for PIC (solid lines) and two-fluid (dashed lines) simulations. Each quantity is plotted as its departure from the corresponding initial value, e.g., $\delta E_b = E_b(t) - E_b(0)$. After an initial adjustment, all quantities decay in time. The kinetic (red lines) and magnetic energy (black lines) show similar behavior but the magnetic energy is smaller in the two-fluid case than in the kinetic simulation, while the kinetic energy is larger in the fluid simulation. A possible reason for this discrepancy could be the absence of viscous-like Pi-D interactions^(57,58) in the fluid case, and the absence of resistive-like behavior in the kinetic case.

The interaction of particles and fields in the PIC simulation enables channels that support dissipation processes. Interchange between flow and thermal energy is essential for physical dissipation, but the two-fluid (incompressible, isothermal) simulation lacks such couplings and therefore all the energy transported from the macro-scale to the smaller scales is artificially removed by viscous and resistive effects. The total variation of the thermal energy ($\delta E_{thi} + \delta E_{the}$) in PIC, and the total variance of the flow energy $-(\delta E_k + \delta E_b)$ in both cases, are also shown in the middle panel of Figure 1 (green and blue lines respectively). The changes δE_{th} and $-(\delta E_k + \delta E_b)$ follow each other almost perfectly for the PIC case, indicating extremely good energy conservation (see also⁶⁸). The change $-(\delta E_k + \delta E_b)$ for the fluid run interestingly follows the PIC values very closely inspite of the differences in quantitative behavior of individual magnetic and

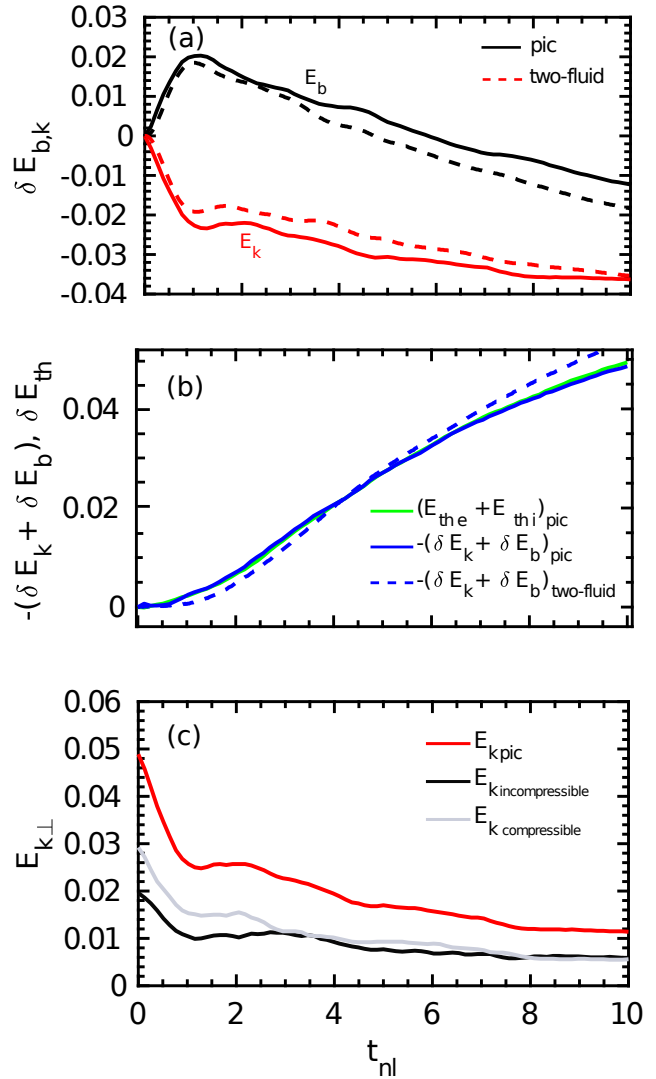


FIG. 1. [Top] (a). Time evolution of the variation in the magnetic energy (black), kinetic flow energy (red) for the full-kinetic simulation (solid lines) and for the two-fluid simulation (dashed line). [Middle] (b). The Variation of the total thermal energy (green) and the negative value of the flow energy dissipation for both simulations (blue). [Bottom] (c) incompressible (black), compressible (gray) and total (red) perpendicular kinetic energy for the PIC simulation.

flow energies. This result suggests that von Karman phenomenology, in which large scale fluctuations control the decay rate, is obtained for both of these cases. .

In addition to thermal couplings, the PIC simulation also contains flow compressions that are clearly absent in the incompressible two-fluid model. The extent of this difference is quantified using a Helmholtz decomposition of the velocity field, separating the solenoidal and irrotational components. These are equivalent to the incompressible ($\hat{\mathbf{u}}_i(k) = (\hat{\mathbf{I}} - \hat{\mathbf{k}}\hat{\mathbf{k}}) \mathbf{u}(k)$) and the compressible part ($\hat{\mathbf{u}}_c(k) = \mathbf{u}(k) - \hat{\mathbf{u}}_i(k)$). The bottom panel of Figure

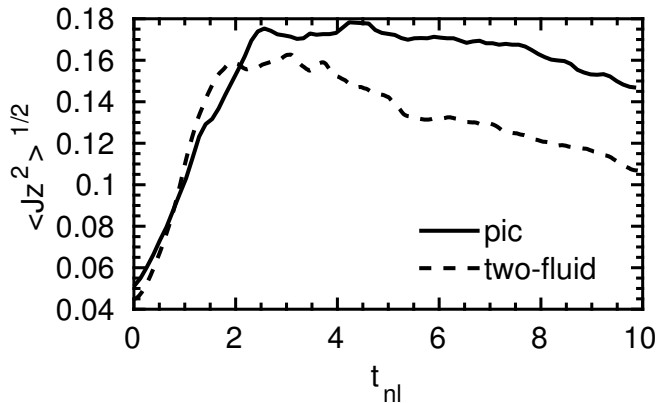


FIG. 2. Time history of the root mean square parallel electric current density (J_z) for the full-kinetic simulation (solid line) and r.m.s electric current density for the two-fluid simulation (dashed line)

1 shows the perpendicular component of the incompressible kinetic energy (black line), the compressible kinetic energy (gray line) and the total kinetic energy (red line) for the PIC simulation. We observe that the compressible component is the dominant part of the kinetic flow energy in the system but both components become of the same order of magnitude a few non-linear times later. The compression of the flow allows a channel where an interchange of energy between incompressible and compressible modes can occur. There is also an energy cascade in each channel. Those effects seem to be very important at sub-proton scales where the compressive coherent structures play a relevant role in the intermittency and the charged particle dynamics.

The root mean square value of the current density in the system is a good indicator of dissipation in plasmas and the increase of this quantity is a consequence of generation of many current sheets mediated by magnetic reconnection. The time evolution of the r.m.s. of the parallel (out of plane) current density J_z is presented in Figure 2. The curves are roughly similar but the peak and late time values of r.m.s current density remain systematically larger in the kinetic PIC simulation. Once the peak is reached in Fig. 2, at about $t = 2t_{nl}$, some current sheets become unstable and the plasma experiences a proliferation of secondary islands or plasmoids due to either turbulent cascade⁶⁹ or due to secondary instability^{20,70}, or both. The generation of a chain of magnetic islands, becomes possible, which in turn could be very important at the electron scales where particles can interact with these electromagnetic structures. Particles with small gyroradii can easily violate the conservation of the adiabatic moments^{71–75} in such interactions. The Figure also shows that the maximum of dissipation is reached early in the fluid simulation. This is a consequence of the fluid viscosity and resistivity that dissipates the energy at a rate slightly faster than in the kinetic simulation.

Cross-sections of the out-of-plane current density are

shown in Figure 3, which depicts the normalized J_z at $t = 3t_{nl}$ for kinetic (Left tpanel) and fluid simulation (right panel). Large current sheets and macroscopic structures are notably similar in these simulations and the signatures of magnetic reconnection are evident in many places in the simulation box. However, the PIC simulation has a more refined small scale structure and some structures are quite different in spatial positions and shape. At this point in the evolution, the system has developed the conditions to the onset of secondary plasmoid formation, through either instability or turbulence cascade effects. As a result, individual small islands or chains of small islands are produced in the interior of large current sheets.

The similarities in the magnetic structure in the simulations also carries over to a statistical description. In Figure 4, we show the perpendicular power spectra of the magnetic field at $t \approx 3t_{nl}$ for the kinetic (solid line) and the two-fluid simulations (dashed line). From the figure one can distinguish breaks in the magnetic spectrum at the particle inertial scales ($k_{\perp}d_i = 1$ and $k_{\perp}d_i = 5$ for ions and electrons respectively).

Once the turbulence is fully developed and the maximum of dissipation is reached, the simulations exhibit the same qualitative behavior at the large scales. The spectral slope shows a Kolmogorov-like power-law in the inertial range for both PIC and two-fluid simulations. A broader inertial range may be obtained in the kinetic simulation only with an intensive use of computational resources. For two-fluid simulations however, we can reproduce powerlaw-like features down to the ion and electron scales, at a remarkably lower computational cost.

Figure 4 also shows that near the proton scales the spectra from both simulations are in good qualitative agreement. The spectral index in this range of scales has a value between $k_{\perp}^{-7/3}$ and $k_{\perp}^{-8/3}$. A universal value of the spectral index at sub-proton scale has not been established and a different value have been observed in numerical simulations with different physical assumptions^{40,76–80}. Variation of the sub-proton range slope is also seen in solar wind observations, usually between -1.75 to -3.75 ^{16,17,25,26}. There is some evidence for the dependence of the spectral index on compressibility (different value for fast and slow wind and a dependence with the plasma beta^{52,70,80,81}), and on cascade rate¹⁷ (steeper spectra for stronger cascade).

The electron scale spectrum is not at all similar in the two simulations, as can be seen in Figure 4. It is worth mentioning that there is no consensus in the community concerning the functional form of the magnetic spectrum at electron scales^{5,23–25}. However the finite electron gyroradii effect must play an important role and those effects are not retained in the two-fluid simulation.

The large-scale structures and the resulting small-scale structures produced by the shrinking of sheets into a smaller-scale magnetic structures is a very important feature in plasma turbulence. The relevance of the coherent structures for particle energization is driven by the

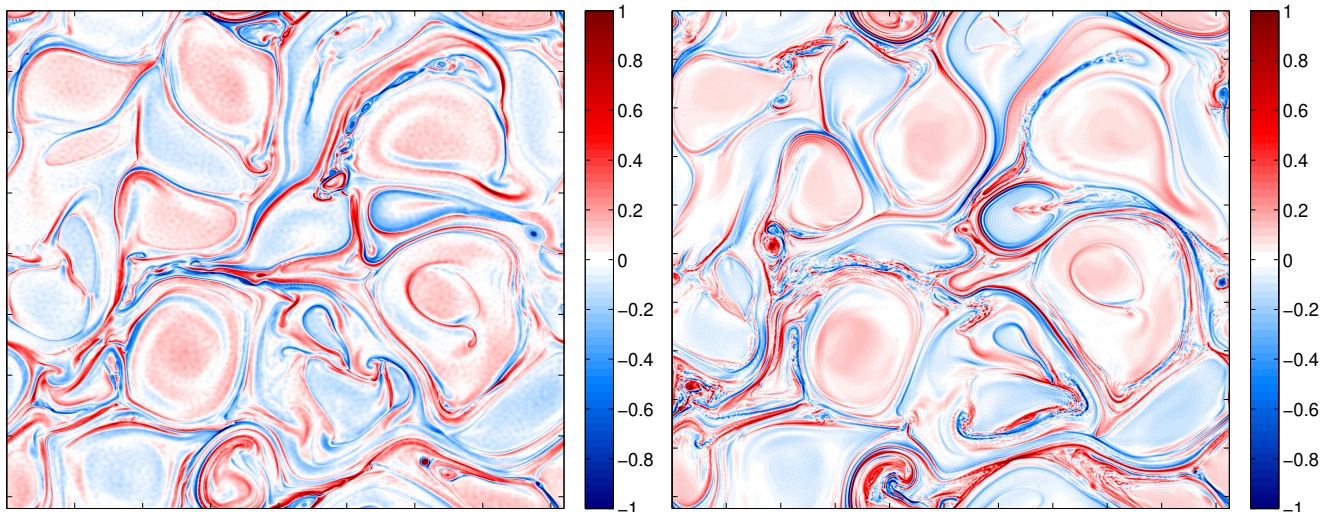


FIG. 3. Contour plot of the out-of-plane normalized electric current density (J_z) at the time of the maximum enstrophy in each simulation ($t \approx 3t_{nl}$). [Left] snapshot of J_z for the full-kinetic simulation. [Right] the same for the two-fluid simulation.

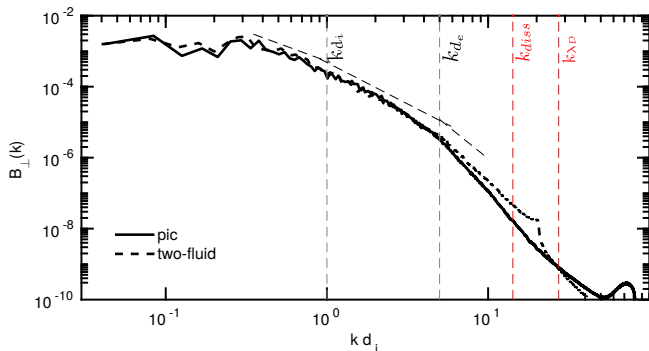


FIG. 4. Energy spectrum of the perpendicular components of the magnetic field at $t \approx 3t_{nl}$ for PIC simulation (solid line) and for the two-fluid simulation (dashed-lines). Vertical gray dashed lines represent the wavenumbers associated with the ion and electron inertial lengths. Red dashed lines represent the smallest scale for each model, dissipation scale (fluid model) and the Debye length (PIC simulation).

electric field that has the capacity to do work on the particles. In order to shed light on the nature of the electric field across scales, we study the contributions to the generalized Ohm's law terms for both types of numerical simulations. Simple scaling analysis can be used to understand the scales at which different terms in Ohm's law become important. However, the exact breakdown of importance of all the terms in parallel and perpendicular components, and across different models is a non-trivial task. We show this breakdown of all the terms in figure 5.

Figure 5 (a) compares contributions to the perpendic-

ular component of the electric field spectrum, from the generalized Ohm's law and from the fluid and kinetic simulations. Top-right panel shows the inductive or MHD term (blue lines), the Hall term (green lines), electron inertia term (black lines). These are shown for both simulations. The pressure contribution is the sum of contributions from the isotropic and the anisotropic part of the pressure tensor (magenta lines), and can be computed only from the kinetic simulation. The inductive term is the largest contribution at the the MHD macroscales and in this range the kinetic and two-fluid simulations are in close agreement. This is expected since the physics of the large scale dynamics is well represented in both simulation models.

Going beyond the proton scale to smaller scales, the inductive term ceases to be dominant, and the Hall term becomes important. The resulting Hall electric field is similar in both simulations up to the wavenumber corresponding to the electron inertial scale. Beyond that, additional contributions in Ohm's law are required.

The perpendicular electric field spectrum from the electron inertia term shows similar spectral shape to the inductive term, but at much lower level. Electron inertial contributions are somewhat stronger in the kinetic simulation than in the two-fluid simulation at sub-proton scales.

The pressure related electric field effect is small at large scales and plays an increasingly important role at sub-proton scales, and it is comparable to the Hall term when approaching the electron inertial length. The most relevant contributions to the pressure term comes from the non-diagonal terms of the pressure tensor which contains the finite electron Larmor radius effects that are neglected in the incompressible two-fluid model. If we do not take into account the pressure effects on the electric

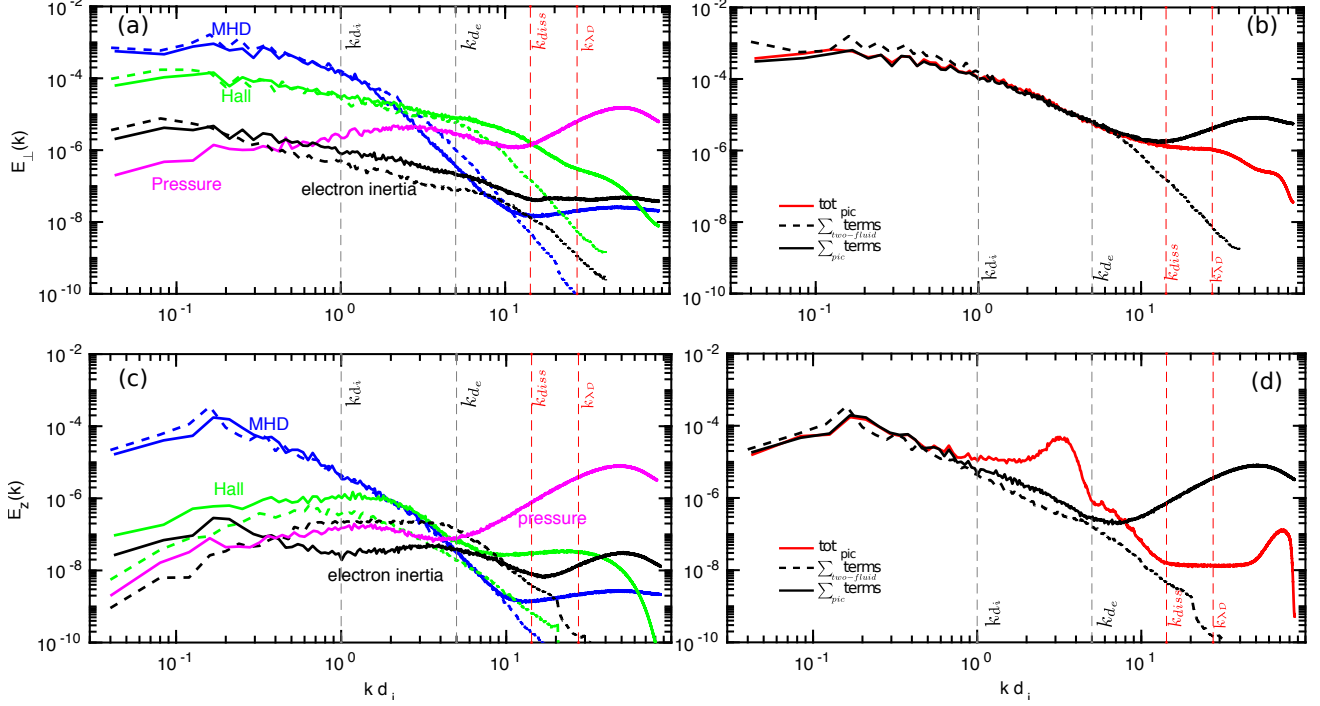


FIG. 5. (*Left-Top.*) (a). Power spectrum of the perpendicular electric field for both simulations. The relevant electric field terms for kinetic simulation (solid lines) and for two-fluid simulation (dashed lines). (*Right-Top.*) (b) Contributions to the total perpendicular electric field due to the terms in the generalized Ohm's law for kinetic simulation and for the two-fluid simulation (black lines) and the total electric field in the PIC simulation by solving Maxwell equations (red line). (*Left-Bottom.*) (c). Spectrum of the parallel component of the electric field for both simulations. The relevant electric field terms for kinetic simulation and for two-fluid simulation with the same line style used in the top panels. (*Right- Bottom.*) (d). Spectrum of the total parallel electric field from the generalized Ohms law for both types of simulations, and from direct output of the PIC simulation. (same line style employed in top panels). Vertical gray dashed lines represent the wavenumbers associated with the ion and electron inertial lengths. Red dashed lines represent the dissipation scale and the Debye length, respectively.

field, the perpendicular component of the total electric field for both simulations is very well correlated at all scales (see the top-right panel or Figure 5 (b)).

The total perpendicular electric field for both simulations at the large MHD scales are similar, with a slightly greater perpendicular electric field spectral density in the two fluid simulation. Moving to scales smaller than the ion inertial length, the two models remain similar, but the kinetic simulation has slightly greater spectral amplitude that could arise from additional kinetic effects that are not contained in the Ohm's law terms we computed. At the electron inertial scale the curves become almost equal, and at still smaller scales the spectral density in the fluid case is heavily suppressed due to resistivity, while the kinetic case indicates an enhancement most likely due to Langmuir oscillations.

Figure 5.(c) depicts the spectrum of the parallel electric field. The most relevant terms of the generalized Ohm's law for this particular direction are the MHD and Hall terms, the pressure effects that only contain the contributions from the divergence of pressure tensor because

the gradient of isotropic pressure cannot be determined in the direction of the guide field due to our 2D domain. Also the resistive electric field is not shown since it is not of physical interest for weakly collisional plasmas, and has no counterpart in the collisionless model that we are studying with the PIC simulation.

Electron inertia term remains smaller than the Hall term down to dissipative/Debye scales in the perpendicular field but for parallel electric field, the inertia term becomes comparable to Hall term just beyond electron scales in PIC. In the fluid case, it supersedes the Hall term at scales much larger than the electron scales. The pressure effects shows relative importance at sub-proton scales, this parallel electric field comes from purely kinetic effects due to the non-gyrotropic contributions of the pressure tensor. Nongyrotropy could play an important role in several different phenomena like magnetic reconnection, particle acceleration and wave-particle interaction. Further, the parallel electric field at kinetic scales looks much different for both simulations despite the relatively good agreement at large scales. The parallel electric field

in PIC simulation shows a significant bump between proton and electron scales. This bump is not explained by any of the terms in Ohm's law and is possibly because of the non-negligible contributions from plasma fluctuations at those scales, an artifact of the unrealistic value of ω_{pe}/ω_{ce} in our PIC simulation. A detailed breakdown of this anomaly is however beyond the scope of present paper and is left for future investigations.

The electron inertial term takes a significant contribution to the parallel electric field at electron scales but it seems those effects are overestimated in the two-fluid model due to the dissipative and resistive effects contained in the calculation of the Ohm's law.

The parallel electric fields would be better studied in the context of 3D simulation instead of the present 2D simulation. The contribution of the parallel electric field is fundamental to the study of turbulent dissipation in plasmas and it seems that we are not correctly resolving the parallel direction either with the two-fluid or with the kinetic simulation.

V. DISCUSSION:

In this paper we have studied plasma turbulence at scales ranging from macroscopic MHD scales to microscopic kinetic scales using two numerical models that differ greatly in their physical content. The plasma descriptions are, first, a two-fluid MHD model that contain Hall and electron inertia effects, and, second, a full kinetic plasma description through Particle-in-Cell simulation.

The comparison of those two different numerical methods is made in the spirit and context of the "*Turbulent dissipation challenge*". Thus, we constructed a comparison of the two physical models with different numerical schemes under the same initial conditions with similar physical and numerical parameters.

Owing to the inherently distinct nature of the models, there are different scales related to each model that the other one cannot retain. An example is the Debye length in the kinetic simulation, which is the smallest scale where the quasi-neutrality condition of the plasma is valid. On the other hand, the smallest scale in the fluid simulation is the dissipative scale where the energy is dissipated by resistive and viscous effects, a scale that is absent in PIC model. With this in mind, we compared the results in the spatio/temporal scales that both models share in common, that is, the energy containing scales (related with the system size) and the proton and electron scales. We have explored some features of the turbulence at different scales and we have found many similarities in the results, including comparisons of overall decay of the energy density, and the generation of small-scale magnetic structures mediated by magnetic reconnection. We also obtained similar magnetic spectra for both simulations which are in good agreement with theoretical and data measurements.

Particularly revealing is the study of kinetic features

of the electric field in the two-fluid and in the PIC simulation. This affords an assessment of the relevance of a given effect in the kinetic range. We have shown that the perpendicular component to the out-of-plane mean magnetic field is dominated by the MHD electric field at the macroscale and compares well in both simulations. At the proton scale, the Hall term becomes dominant. This part of the electric field is important for small scale structures that naturally appear in the simulation, for example, in the formation of plasmoids that arise in unstable current sheets. The pressure effects are relevant at sub-proton scales with significant contributions from the non-diagonal terms of the pressure tensor that contains the electron finite larmor effects. Those effects are not retained in the incompressible two-fluid model.

The comparison of the electric field between these two types of simulations may help us understand the capacity of the fluid description to retain effects that appear at kinetic scales. Indeed for certain problems the fluid model, that takes into account some kinetic effects, may be the optimal choice. For example, the in-plane electric field is well described by the two-fluid model in some part of the kinetic range although it lacks pressure gradient effects.

However, the parallel component is not well resolved in the 2D computational domain we used here. In addition, the two-fluid simulation does not resolve correctly the microphysics in the parallel direction, and the enhancement of electric field at kinetic scales revealed in the kinetic simulation is not obtained with this model. The parallel electric field plays a significant role in the energy dissipation in plasmas as it mediates the wave-particle interaction through Landau damping and other phenomena that are lacking in this two-fluid model. Clearly in order to understand the whole system 3D simulations are required, which is certainly expensive and large computational resources must be needed to simulate a system size with a representative number of particles in the kinetic simulation. Tiny 3D boxes are not realistic for most applications (see e.g.,⁶⁵) and large 3D PIC simulations are extremely expensive. Hence a full comparison between fully 3D kinetic and fluid simulations is deferred to the future.

The connection of the fluid and kinetic descriptions is relevant for understanding plasma dynamics, due to the need of more efficient tools to resolve the huge range of scales that exist simultaneously in a plasma. This paper has provided a modest step forward in this direction, providing quantitative insights concerning the physics retained in two models: a kinetic simulation, which is more complete and more expensive to run, and a two-fluid simulation which is much less computationally demanding and which in some cases resolves all the scales that are needed. It also could open the door to a new generation of hybrid codes that contain both fluid and kinetic model in its base, see for example Bai et al. (2015)⁸².

ACKNOWLEDGMENTS

C.A.G and P.D. acknowledge support from grants UBACyT No. 20020110200359 and 20020100100315, and from grants PICT No. 2011-1529, 2011-1626, and 2011-0454. TNP was supported by the NSF SHINE grant AGS-1460130. W.H.M. was partially supported by NASA LWS-TRT grant NNX15AB88G, Grand Challenge Research grant NNX14AI63G, and the Solar Probe Plus mission through the Princeton ISOIS. C.A.G acknowledges the support and hospitality during his visit to University of Delaware.

- ¹Kolmogorov, A. *Akademiia Nauk SSSR Doklady* **1941**, *30*, 301–305.
- ²Coleman, P. J., Jr. *ApJ* **1968**, *153*, 371.
- ³Goldstein, M. L.; Roberts, D. A.; Matthaeus, W. H. *Annual Review of Astronomy and Astrophysics* **1995**, *33*, 283–325.
- ⁴Bruno, R.; D’Amicis, R.; Bavassano, B.; Carbone, V.; Sorriso-Valvo, L. **2007**, *55*, 2233–2238.
- ⁵Alexandrova, O.; Mangeney, A.; Maksimovic, M.; Cornilleau-Wehrlin, N.; Bosqued, J.-M.; André, M. *Journal of Geophysical Research: Space Physics* **2006**, *111*, n/a–n/a, A12208.
- ⁶Perri, S.; Goldstein, M. L.; Dorelli, J. C.; Sahraoui, F. *Phys. Rev. Lett.* **2012**, *109*, 191101.
- ⁷Perrone, D.; Alexandrova, O.; Mangeney, A.; Maksimovic, M.; Lacombe, C.; Rakoto, V.; Kasper, J. C.; Jovanovic, D. *The Astrophysical Journal* **2016**, *826*, 196.
- ⁸Bruno, R.; Carbone, V.; Veltri, P.; Pietropaolo, E.; Bavassano, B. **2001**, *49*, 1201–1210.
- ⁹Greco, A.; Matthaeus, W. H.; D’Amicis, R.; Servidio, S.; Dmitruk, P. *The Astrophysical Journal* **2012**, *749*, 105.
- ¹⁰Zhdankin, V.; Boldyrev, S.; Mason, J.; Perez, J. C. *Phys. Rev. Lett.* **2012**, *108*, 175004.
- ¹¹Greco, A.; Chuychai, P.; Matthaeus, W. H.; Servidio, S.; Dmitruk, P. *Geophysical Research Letters* **2008**, *35*, n/a–n/a, L19111.
- ¹²Tessein, J. A.; Matthaeus, W. H.; Wan, M.; Osman, K. T.; Ruffolo, D.; Giacalone, J. *The Astrophysical Journal Letters* **2013**, *776*, L8.
- ¹³Tessein, J. A.; Ruffolo, D.; Matthaeus, W. H.; Wan, M.; Giacalone, J.; Neugebauer, M. *The Astrophysical Journal* **2015**, *812*, 68.
- ¹⁴Dmitruk, P.; Matthaeus, W. H.; Seenu, N. *The Astrophysical Journal* **2004**, *617*, 667.
- ¹⁵González, C. A.; Dmitruk, P.; Mininni, P. D.; Matthaeus, W. H. *The Astrophysical Journal* **2017**, *850*, 19.
- ¹⁶Leamon, R. J.; Matthaeus, W. H.; Smith, C. W.; Wong, H. K. *The Astrophysical Journal Letters* **1998**, *507*, L181.
- ¹⁷Smith, C. W.; Hamilton, K.; Vasquez, B. J.; Leamon, R. J. *The Astrophysical Journal Letters* **2006**, *645*, L85.
- ¹⁸Cerri, S.; Kunz, M.; Califano, F. *The Astrophysical Journal Letters* **2018**, *856*, L13.
- ¹⁹Vech, D.; Mallet, A.; Klein, K. G.; Kasper, J. C. *The Astrophysical Journal Letters* **2018**, *855*, L27.
- ²⁰Loureiro, N. F.; Boldyrev, S. *ArXiv e-prints* **2018**,
- ²¹Alexandrova, O.; Lacombe, C.; Mangeney, A.; Grappin, R.; Maksimovic, M. *The Astrophysical Journal* **2012**, *760*, 121.
- ²²Parashar, T. N.; Salem, C.; Wicks, R. T.; Karimabadi, H.; Gary, S. P.; Matthaeus, W. H. *Journal of Plasma Physics* **2015**, *81*, 905810513.
- ²³Alexandrova, O.; Saur, J.; Lacombe, C.; Mangeney, A.; Mitchell, J.; Schwartz, S. J.; Robert, P. *Phys. Rev. Lett.* **2009**, *103*, 165003.
- ²⁴Sahraoui, F.; Huang, S. Y.; Belmont, G.; Goldstein, M. L.; Réтино, A.; Robert, P.; Patoul, J. D. *The Astrophysical Journal* **2013**, *777*, 15.
- ²⁵Sahraoui, F.; Goldstein, M. L.; Belmont, G.; Canu, P.; Rezeau, L. *Phys. Rev. Lett.* **2010**, *105*, 131101.
- ²⁶Salem, C. S.; Howes, G. G.; Sundkvist, D.; Bale, S. D.; Chaston, C. C.; Chen, C. H. K.; Mozer, F. S. *The Astrophysical Journal Letters* **2012**, *745*, L9.
- ²⁷Saito, S.; Gary, S. P.; Narita, Y. *Physics of Plasmas* **2010**, *17*, 122316.
- ²⁸Narita, Y.; Gary, S. P. *Annales Geophysicae* **2010**, *28*, 597–601.
- ²⁹Podesta, J. J.; Gary, S. P. *The Astrophysical Journal* **2011**, *734*, 15.
- ³⁰Hughes, R. S.; Gary, S. P.; Wang, J.; Parashar, T. N. *The Astrophysical Journal Letters* **2017**, *847*, L14.
- ³¹Grošelj, D.; Mallet, A.; Loureiro, N. F.; Jenko, F. *Phys. Rev. Lett.* **2018**, *120*, 105101.
- ³²Cerri, S. S.; Califano, F.; Jenko, F.; Told, D.; Rincon, F. *The Astrophysical Journal Letters* **2016**, *822*, L12.
- ³³Mozer, F. S.; Chen, C. H. K. *The Astrophysical Journal Letters* **2013**, *768*, L10.
- ³⁴Bale, S. D.; Kellogg, P. J.; Mozer, F. S.; Horbury, T. S.; Reme, H. *Phys. Rev. Lett.* **2005**, *94*, 215002.
- ³⁵Matteini, L.; Alexandrova, O.; Chen, C. H. K.; Lacombe, C. *MNRAS* **2017**, *466*, 945–951.
- ³⁶Schekochihin, A. A.; Cowley, S. C.; Dorland, W.; Hammett, G. W.; Howes, G. G.; Quataert, E.; Tatsuno, T. *The Astrophysical Journal Supplement Series* **2009**, *182*, 310.
- ³⁷Quataert, E. *The Astrophysical Journal* **1998**, *500*, 978.
- ³⁸Ghosh, S.; Goldstein, M. L. *Journal of Plasma Physics* **1997**, *57*, 129–154.
- ³⁹Das, A.; Diamond, P. H. *Physics of Plasmas* **2000**, *7*, 170–177.
- ⁴⁰Shaikh, D. *Monthly Notices of the Royal Astronomical Society* **2009**, *395*, 2292–2298.
- ⁴¹Andrés, N.; Gonzalez, C.; Martin, L.; Dmitruk, P.; Gómez, D. *Physics of Plasmas* **2014**, *21*, 122305.
- ⁴²Yajima, N. *Progress of Theoretical Physics* **1966**, *36*, 1–16.
- ⁴³Ghosh, S.; Siregar, E.; Roberts, D. A.; Goldstein, M. L. *Journal of Geophysical Research: Space Physics* **101**, 2493–2504.
- ⁴⁴Hammett, G. W.; Perkins, F. W. *Phys. Rev. Lett.* **1990**, *64*, 3019–3022.
- ⁴⁵Passot, T.; Sulem, P. L. *Physics of Plasmas* **2004**, *11*, 5173–5189.
- ⁴⁶Vencels, J.; Delzanno, G. L.; Manzini, G.; Markidis, S.; Peng, I. B.; Roytershteyn, V. *Journal of Physics: Conference Series* **2016**, *719*, 012022.
- ⁴⁷Juno, J.; Hakim, A.; TenBarge, J.; Shi, E.; Dorland, W. *Journal of Computational Physics* **2018**, *353*, 110 – 147.
- ⁴⁸Birdsall, C. K.; Langdon, A. B. *Plasma Physics via Computer Simulation (Series in Plasma Physics)*, 1st ed.; Taylor & Francis, 2004.
- ⁴⁹Hockney, R. W.; Eastwood, J. W. *Computer Simulation Using Particles*; Taylor & Francis, 1989.
- ⁵⁰Valentini, F.; Trávníček, P.; Califano, F.; Hellinger, P.; Mangeney, A. *Journal of Computational Physics* **2007**, *225*, 753 – 770.
- ⁵¹Cerri, S. S.; Franci, L.; Califano, F.; Landi, S.; Hellinger, P. *Journal of Plasma Physics* **2017**, *83*, 705830202.
- ⁵²Grošelj, D.; Cerri, S. S.; Bañón Navarro, A.; Willmott, C.; Told, D.; Loureiro, N. F.; Califano, F.; Jenko, F. *ApJ* **2017**, *847*, 28.
- ⁵³Stanier, A.; Daughton, W.; Simakov, A. N.; Chacón, L.; Le, A.; Karimabadi, H.; Ng, J.; Bhattacharjee, A. *Physics of Plasmas* **2017**, *24*, 022124.
- ⁵⁴Franci, L.; Cerri, S. S.; Califano, F.; Landi, S.; Papini, E.; Verdini, A.; Matteini, L.; Jenko, F.; Hellinger, P. *The Astrophysical Journal Letters* **2017**, *850*, L16.
- ⁵⁵Pezzi, O.; Parashar, T. N.; Servidio, S.; Valentini, F.; Vásconez, C. L.; Yang, Y.; Malara, F.; Matthaeus, W. H.; Veltri, P. *Journal of Plasma Physics* **2017**, *83*, 705830108.
- ⁵⁶Klein, K. G.; Howes, G. G. *The Astrophysical Journal Letters* **2016**, *826*, L30.
- ⁵⁷Yang, Y.; Matthaeus, W. H.; Parashar, T. N.; Wu, P.; Wan, M.; Shi, Y.; Chen, S.; Roytershteyn, V.; Daughton, W. *PRE* **2017**,

- 95, 061201.
- ⁵⁸Yang, Y.; Matthaeus, W. H.; Parashar, T. N.; Wu, P.; Wan, M.; Shi, Y.; Chen, S.; Roytershteyn, V.; Daughton, W. *Phys. Rev. E* **2017**, *95*, 061201.
- ⁵⁹Howes, G. G.; Klein, K. G.; Li, T. C. *Journal of Plasma Physics* **2017**, *83*, 705830102.
- ⁶⁰Chasapis, A.; Yang, Y.; Matthaeus, W. H.; Parashar, T. N.; Haggerty, C. C.; Burch, J. L.; Moore, T. E.; Pollock, C. J.; Dorelli, J.; Gershman, D. J.; Torbert, R. B.; Russell, C. T. *The Astrophysical Journal* **2018**, *862*, 32.
- ⁶¹Vasylinas, V. M. *Annales Geophysicae* **2005**, *23*, 1347–1354.
- ⁶²Krishnaswami, G. S.; Sachdev, S.; Thyagaraja, A. *ArXiv e-prints* **2017**,
- ⁶³Che, H.; Schiff, C.; Le, G.; Dorelli, J. C.; Giles, B. L.; Moore, T. E. *Physics of Plasmas* **2018**, *25*, 032101.
- ⁶⁴Zeiler, A.; Biskamp, D.; Drake, J. F.; Rogers, B. N.; Shay, M. A.; Scholer, M. *Journal of Geophysical Research (Space Physics)* **2002**, *107*, 1230.
- ⁶⁵Parashar, T. N.; Matthaeus, W. H.; Shay, M. A.; Wan, M. *The Astrophysical Journal* **2015**, *811*, 112.
- ⁶⁶Turner, M. M. *Physics of Plasmas* **2006**, *13*, 033506.
- ⁶⁷Haggerty, C. C.; Parashar, T. N.; Matthaeus, W. H.; Shay, M. A.; Yang, Y.; Wan, M.; Wu, P.; Servidio, S. *Physics of Plasmas* **2017**, *24*, 102308.
- ⁶⁸Parashar, T. N.; Matthaeus, W. H.; Shay, M. A. *arXiv preprint arXiv:1807.11371* **2018**,
- ⁶⁹Wan, M.; Matthaeus, W.; Roytershteyn, V.; Parashar, T.; Wu, P.; Karimabadi, H. *Physics of Plasmas* **2016**, *23*, 042307.
- ⁷⁰Cerri, S. S.; Califano, F. *New Journal of Physics* **2017**, *19*, 025007.
- ⁷¹Dahlin, J. T.; Drake, J. F.; Swisdak, M. *Physics of Plasmas* **2014**, *21*, 092304.
- ⁷²Dalena, S.; Greco, A.; Rappazzo, A. F.; Mace, R. L.; Matthaeus, W. H. *Phys. Rev. E* **2012**, *86*, 016402.
- ⁷³le Roux, J. A.; Zank, G. P.; Webb, G. M.; Khabarova, O. *The Astrophysical Journal* **2015**, *801*, 112.
- ⁷⁴Zank, G. P.; le Roux, J. A.; Webb, G. M.; Dosch, A.; Khabarova, O. *ApJ* **2014**, *797*, 28.
- ⁷⁵Dahlin, J. T.; Drake, J. F.; Swisdak, M. *Physics of Plasmas* **2017**, *24*, 092110.
- ⁷⁶Biskamp, D.; Schwarz, E.; Zeiler, A.; Celani, A.; Drake, J. F. *Physics of Plasmas* **1999**, *6*, 751–758.
- ⁷⁷Howes, G. G.; Dorland, W.; Cowley, S. C.; Hammett, G. W.; Quataert, E.; Schekochihin, A. A.; Tatsuno, T. *Phys. Rev. Lett.* **2008**, *100*, 065004.
- ⁷⁸Passot, T.; Henri, P.; Laveder, D.; Sulem, P.-L. *The European Physical Journal D* **2014**, *68*, 207.
- ⁷⁹Wan, M.; Matthaeus, W. H.; Karimabadi, H.; Roytershteyn, V.; Shay, M.; Wu, P.; Daughton, W.; Loring, B.; Chapman, S. C. *Phys. Rev. Lett.* **2012**, *109*, 195001.
- ⁸⁰Franci, L.; Landi, S.; Matteini, L.; Verdini, A.; Hellinger, P. *The Astrophysical Journal* **2016**, *833*, 91.
- ⁸¹Bruno, R.; Trenchi, L.; Telloni, D. *The Astrophysical Journal Letters* **2014**, *793*, L15.
- ⁸²Bai, X.-N.; Caprioli, D.; Sironi, L.; Spitkovsky, A. *The Astrophysical Journal* **2015**, *809*, 55.
- ⁸³Perrone, D.; Valentini, F.; Servidio, S.; Dalena, S.; Veltri, P. *ApJ* **2013**, *762*, 99.
- ⁸⁴Yajima, N. *Progress of Theoretical Physics* **1966**, *36*, 1–16.